Proportional derivative based stabilizing control of paralleled grid converters with cables in renewable power plants

Wang, Xiongfei; Blaabjerg, Frede; Loh, Poh Chiang

Published in:
Proceedings of the 2014 IEEE Energy Conversion Congress and Exposition (ECCE)

DOI (link to publication from Publisher):
10.1109/ECCE.2014.6954075

Publication date:
2014

Document Version
Early version, also known as pre-print

Proportional Derivative Based Stabilizing Control of Paralleled Grid Converters with Cables in Renwable Power Plants

Xiongfei Wang, Frede Blaabjerg, Poh Chiang Loh
Department of Energy Technology, Aalborg University, Aalborg, Denmark
xwa@et.aau.dk, fbl@et.aau.dk, pcl@et.aau.dk

***Abstract*—Resonant interactions of grid-connected converters with each other and with cable capacitance are challenging the stability and power quality of renewable energy sources based power plants. This paper addresses the instability of current control of converters with the multiple resonance frequencies consisting in *LCL* filters and cables. Both grid and converter current controls are analyzed. The frequency region, within which the system may be destabilized, is identified by means of the impedance-based stability analysis and frequency-domain passivity theory. A proportional derivative control strategy is then proposed to stabilize the system. Simulation case studies on four paralleled grid converters and experimental tests for two paralleled grid converters are carried out to validate the performance of the proposed control.**

I. INTRODUCTION

The share of renewable energy sources, particularly wind turbines and photovoltaic panels, has been keeping a rapid growth in electrical grids. The large renewable energy based power generation plants are emerging into power grids [1]. A widespread use of power electronics converters in renewable energy sources furnishes full controllability and flexibility for renewable power plants. However, harmonics generated from high-frequency switching operation of converters may make influence on other devices and even trigger resonances [2]. Using *LCL* filters for switching harmonics attenuation may lead to the instability of grid converters and subsequent resonance propagation in power plants [3]. This challenge is getting worse with the multiple resonance frequencies caused by power transmission cables and other paralleled converters [4]. Hence, the control of grid converters with the multiple resonance frequencies instead of single *LCL* filter resonance becomes important to keep the stability and power quality of renewable power plants.

Generally, the stability of grid converters is dependent on multiple control loops, including the current control loop, active/reactive power control loops, and grid synchronization loop [5]. Since the bandwidth of the power control and grid synchronization loops are usually well below the resonance frequencies of *LCL* filters and cables, the current control loop becomes more sensitive to resonance peaks [6].

The interaction of current control loop with single *LCL* resonance frequency has been thoroughly discussed in many research works [6]-[10]. A number of passive dampers [7] or active damping control methods [8]-[10] have been reported to address the *LCL* resonance. However, only a few of them can be found for the stability of current control with multiple resonance frequencies [4], [9]. In [4], the active damping control with the cascade notch filters in series with current controller is introduced to stabilize the system. However, it is worth noting that the multiple resonance frequencies do not imply the appearance of multiple oscillations in the current control loop. To clarify the instability effect of multiple resonance frequencies, the numerical analysis with pole zero map is reported in [9], the analytical approach is however missing. Moreover, the use of notch filters for resonance damping is sensitive to the parameter uncertainties, which has to be adaptive to the varied resonance frequencies [10].

This paper addresses the resonant interactions among the current control of grid converters and the multiple resonance frequencies caused by cable capacitances and the paralleled converters. Both grid current and converter current control are analyzed considering the effect of the digital computation and Pulse Width Modulation (PWM) delays. The frequency region for unstable current control is identified by means of impedance-based analysis and frequency-domain passivity theory [6], [15]-[16]. To stabilize the current control with the multiple resonance frequencies, an active damping control strategy based on a backward Euler derivative controller is proposed. For converter current control, the Euler derivative controller is used with an additional zero compensation. For grid current control, the derivative controller is implemented with a positive feedback. Simulations of four grid converters interconnected with power cables and laboratory tests of two paralleled converters validate the proposed approach.

This work was supported by European Research Council (ERC) under the European Union's Seventh Framework Program (FP/2007-2013)/ERC Grant Agreement [321149-Harmony].

978-1-4799-5776-7/14/$31.00 ©2014 IEEE

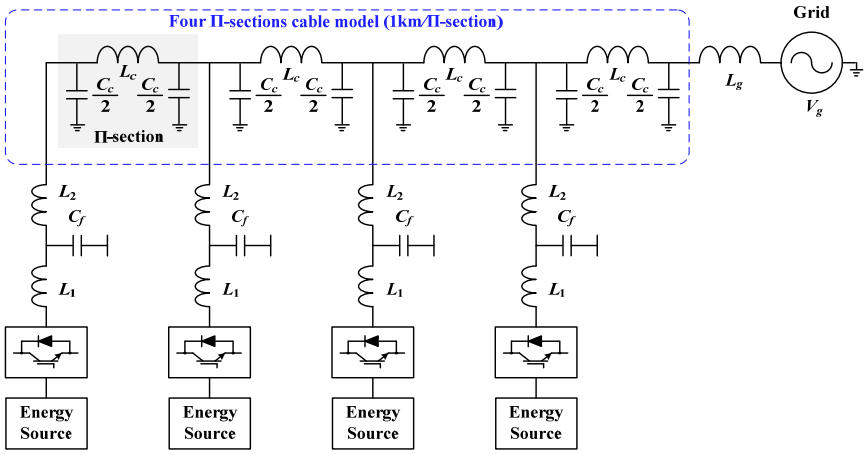

Fig. 1. Simplified one-line diagram of a distribution feeder with four grid converters.

II. System Description

Fig. 1 illustrates a simplified one-line diagram of a cable-based distribution feeder in a renewable power plant. Four renewable energy sources interfaced with grid converters are interconnected by the 1km Π-equivalent cable models. *LCL* filters are used to attenuate switching harmonics produced by converters. Table I gives the main circuit parameters of the system. For simplicity, the converters are assumed to have the same parameters, and their DC-link voltages are constant.

Fig. 2 shows a general control diagram of the converter. The Phase-Locked Loop (PLL) is used to synchronize with the Point of Connection (PoC) voltage. To avoid unwanted low-frequency instabilities induced by grid synchronization, the PLL is designed to have a lower bandwidth than the grid fundamental frequency [11]-[13]. Both the converter current i_1 and grid current i_2 can be controlled, whose diagrams are detailed in Fig. 3. $G_c(s)$ is the current controller implemented with a Proportional Resonant (PR) controller. $G_d(s)$ denotes the computation and Pulse Width Modulation (PWM) delays in the digital control system [14].

$$G_c(s) = k_p + \frac{k_i s}{s^2 + \omega_1^2} \tag{1}$$

$$G_d(s) = e^{-1.5T_s s} \tag{2}$$

where $\omega_1 = 2\pi f_1$, f_1 is the grid fundamental frequency, T_s is the sampling period of control system.

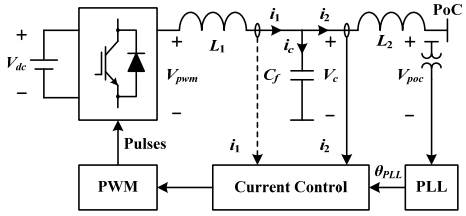

Fig. 2. General diagram of grid converter with single-loop current control.

TABLE I. Main Circuit Parameters

Symbol	Electrical Constant	Value
V_g	Grid voltage	400 V
f_1	Grid fundamental frequency	50 Hz
L_g	Grid inductance	2 mH
f_{sw}	Converter switching frequency	10 kHz
f_s	Converter sampling frequency	10 kHz
V_{dc}	Converter DC-link voltage	750 V
L_1	*LCL* filter - converter-side inductor	2.7 mH
L_2	*LCL* filter - grid-side inductor	0.9 mH
C_f	*LCL* filter - capacitor	9.4 μF
L_c	Cable inductance	0.48 mH/km
C_c	Cable capacitance	0.46 μF/km
r_c	Cable resistance	0.025 Ω/km

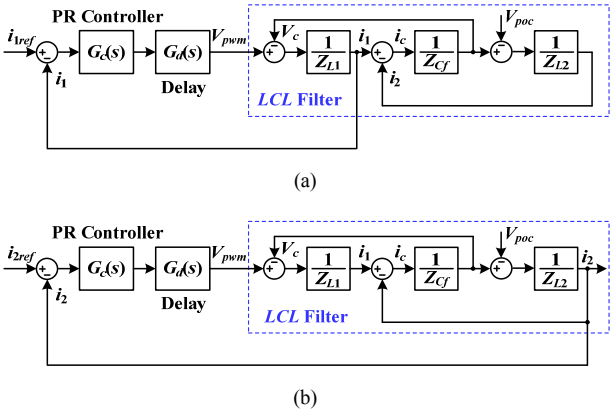

Fig. 3. Block diagrams of current control of grid converters. (a) Converter current control loop. (b) Grid current control loop.

III. IMPEDANCE-BASED STABILITY ANALYSIS

A. Modeling of Grid Converters

Fig. 4 shows the Norton equivalent models of converter and grid current control loops at the PoC of converters. To preserve the electric property at the PoC of the converter, the equivalent model of converter current control is derived at the filter capacitor, as shown in Fig. 4 (a), where the "plant" of control loop is the converter-side inductor L_1. Thus, the terminal behavior of converter current control at the PoC can be derived in the following

$$T_1 = G_c G_d Y_{1p}, \quad Y_{1p} = Y_{1o} = \frac{1}{Z_{L1}} \tag{3}$$

$$G_{1cl} = \frac{T_1}{1+T_1}, \quad Y_{1c} = \frac{Y_{1o}}{1+T_1} = \frac{1}{\frac{1}{Y_{1o}} + \frac{1}{Y_{1d}}}, \quad Y_{1d} = \frac{1}{G_c G_d} \tag{4}$$

$$i_1 = \frac{Z_{L2} + Z_{Cf}}{Y_{1c} Z_{Cf} Z_{L2} + Z_{L2} + Z_{Cf}} G_{1cl} i_{1ref} - \frac{Y_{1c} Z_{Cf}}{Y_{1c} Z_{Cf} Z_{L2} + Z_{L2} + Z_{Cf}} V_{poc} \tag{5}$$

where T_1 and G_{1cl} are the open-loop and closed-loop gains of control loop, respectively. Y_{1o} and Y_{1c} are the open-loop and closed-loop output admittances of control loop, respectively. Y_{1p} is the transfer function derived from the converter voltage to converter current. From (4), it is seen that the closed-loop output admittance Y_{1c} is equivalent to the open-loop output admittance Y_{1o} in series with an admittance introduced by the control loop, i.e. $Y_{1d} = 1/(G_c G_d)$.

In contrast, the terminal behavior of grid current control loop is directly equivalent to a Norton circuit, as shown in Fig. 4 (b), and the "plant" of control loop is the *LCL* filter.

$$\begin{aligned} Y_{2p} &= \left.\frac{i_2}{V_{pwm}}\right|_{V_{poc}=0} = \frac{Z_{Cf}}{Z_{Cf} Z_{L1} + Z_{L2} Z_{L1} + Z_{Cf} Z_{L2}} \\ Y_{2o} &= \left.\frac{i_2}{V_{poc}}\right|_{V_{pwm}=0} = \frac{Z_{Cf} + Z_{L1}}{Z_{Cf} Z_{L1} + Z_{L2} Z_{L1} + Z_{Cf} Z_{L2}} \end{aligned} \tag{6}$$

where Y_{2p} is the transfer function from the converter voltage to grid current, Y_{2o} is the open-loop output admittance. Thus, the terminal behavior of grid current control is derived as

$$T_2 = G_c G_d Y_{2p}, \quad G_{2cl} = \frac{T_2}{1+T_2} \tag{7}$$

$$Y_{2c} = \frac{Y_{2o}}{1+T_2} = \frac{1}{\frac{1}{Y_{2o}} + \frac{1}{Y_{2d}}}, \quad Y_{2d} = \frac{Z_{Cf} + Z_{L1}}{G_c G_d Z_{Cf}} \tag{8}$$

where T_2 and G_{2cl} are the open-loop and closed-loop gains of grid current control loop, respectively. Y_{2c} is the closed-loop output admittance, which is similar to (4), is equivalent to a series connection of the open-loop output admittance and an admittance introduced by the control loop Y_{2d}.

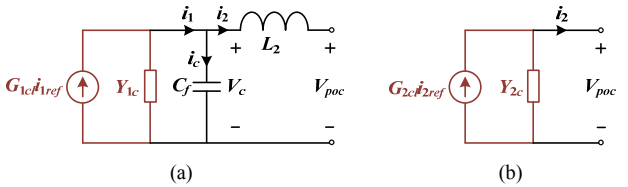

Fig. 4. Norton equivalent models of grid converters. (a) Converter current control. (b) Grid current control.

B. Passivity of Current Control

Given a linear, continuous system $G(s)$, the passivity in the frequency-domain is defined as follows [15]:

1) $G(s)$ has no Right Half-Plane (RHP) poles.

2) $\mathrm{Re}\{G(j\omega)\} \geq 0 \Leftrightarrow \arg\{G(j\omega)\} \in [-90^\circ, 90^\circ], \ \forall \omega > 0$.

This is an important property of a dynamical system, which has been applied to the design of current controller for grid-connected converters [6], and the stability assessment of the cascaded DC-DC converters [16]. It has been shown that if each subsystem in an interconnected system is passive, the whole system will be stable [15]. Hence, if the closed-loop output admittances Y_{1c} and Y_{2c} have non-negative real parts, the interactions among the current control and the resonant grids will be stable, since cables and *LCL* filters are passive.

However, from (4) and (8), it can be found that the time delay in digital control system, denoted as G_d, will introduce a negative conductance into the admittances Y_{1d} and Y_{2d}, and consequently the closed-loop output admittances Y_{1c} and Y_{2c}. They are illustrated as follows

$$Y_{1d} = \frac{1}{k_p} e^{j1.5\omega T_s} = \frac{1}{k_p}\left[\cos(1.5T_s\omega) + j\sin(1.5T_s\omega)\right] \tag{9}$$

$$Y_{2d} = \frac{1 - L_1 C_f \omega^2}{k_p} e^{j1.5T_s\omega} = \frac{1 - L_1 C_f \omega^2}{k_p}\left[\cos(1.5T_s\omega) + j\sin(1.5T_s\omega)\right] \tag{10}$$

where (1) and (2) are substituted into the admittances Y_{1d} and Y_{2d}, and the resonant controller in (1) is nullified since it only takes effect at the fundamental frequency. Based on (9), it is seen that Y_{1d} yields a negative conductance between the one sixth of the sampling frequency and the Nyquist frequency ($f_s/6$, $f_s/2$). From (10), it can be derived that Y_{2d} possesses a negative conductance between the resonance frequency of L_1 and C_f and $f_s/6$.

C. Impedance-Based Stability Analysis

To illustrate first the basic principle of impedance-based stability analysis, the stability of converter current control is

analyzed in the following based on Fig. 4 (a). By rearranging (5), the closed-loop response of converter current i_1 can be expressed as

$$i_1 = \frac{1}{1+Y_{1c}/Y_{L2C}} G_{1cl} i_{1ref} - \frac{Y_{1c}/Y_{L2C}}{1+Y_{1c}/Y_{L2C}} \frac{V_{poc}}{Z_{L2}} \tag{11}$$

where Y_{L2C} is the admittance of paralleling filter capacitor C_f and grid-side inductor L_2, $Y_{L2C} = (Z_{L2}+Z_{Cf})/(Z_{L2}Z_{Cf})$. Thus, the stability of converter current control is dependent on a minor feedback loop composed by the admittance ratio Y_{1c}/Y_{L2C}, in addition to the closed-loop gain G_{1cl}.

Fig. 5 shows the frequency responses for the open-loop gain T_1, and the admittances Y_{1c} and Y_{L2C}. The proportional gain of current controller is designed with the 45° of phase margin, as shown in Fig. 5 (a). Hence, G_{1cl} is stable and the system stability is determined by the minor feedback loop. Fig. 5 (b) plots the frequency responses of the admittances Y_{1c} and Y_{L2C}, where the phase difference at the intersection points of their magnitude responses give the phase margin of the minor feedback loop. A negative phase margin is resulted if the phase difference is higher than 180°. It is seen from Fig. 5 (b) that the phase of Y_{1c} is out of [-90°, 90°] between $f_s/6$ and $f_s/2$, which verifies (9). Moreover, an intersection point falls in this frequency range, where the phase difference indicates a negative phase margin of converter current control loop. Hence, the frequency range, within which the phase of the closed-loop output admittance has a negative conductance, is the region that the system may be destabilized.

Then, substituting the Norton equivalent models for grid converters in Fig. 1, the equivalent circuits of the distribution feeder can be drawn in Fig. 6. Since converter current control is unstable at the PoC, only the interaction among the grid current control of converters and cables shown in Fig. 6 (b) is analyzed with the impedance-based ratio derived in (12). The equivalent circuit shown in Fig. 6 (a) will be discussed later with the proposed stabilizing control method.

$$T_{2m} = Y_{2c}/Y_{2load} \tag{12}$$

where Y_{2load} is the equivalent load admittance derived at the PoC of the converter which is farthest from grid. T_{2m} is the open-loop gain of the minor feedback loop.

Fig. 7 plots the frequency responses for the open-loop gain T_2 and the closed-loop output admittances Y_{2c}. A stable terminal behavior at the PoC is observed in Fig. 7 (a). This is due to the inherent damping effect of time delay in the digital

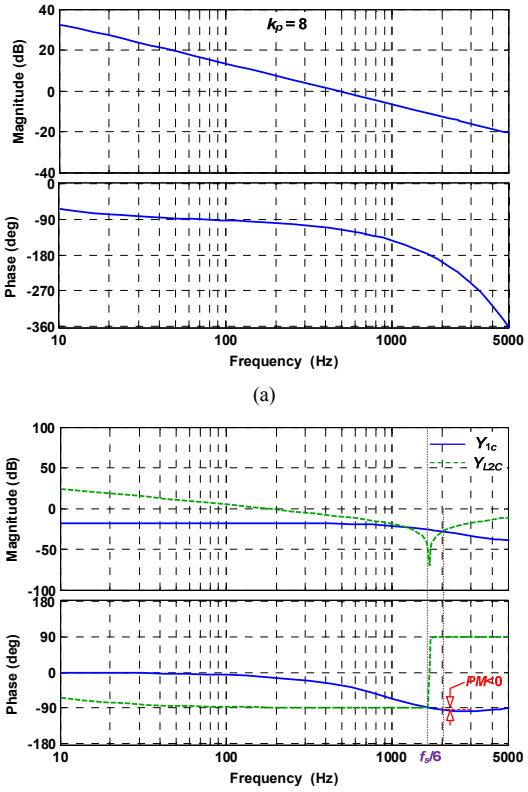

Fig. 5. Frequency responses of converter current control loop. (a) Open-loop gain T_1. (b) Closed-loop output admittance Y_{1c} and the admittance Y_{L2C}.

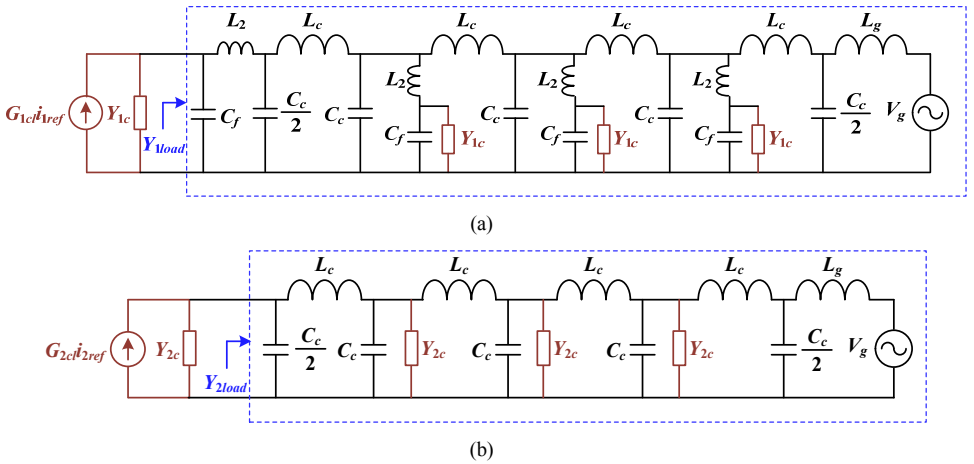

Fig. 6. Impedance-based equivalent circuits of the distribution feeder with four grid converters. (a) Converter current control. (b) Grid current control.

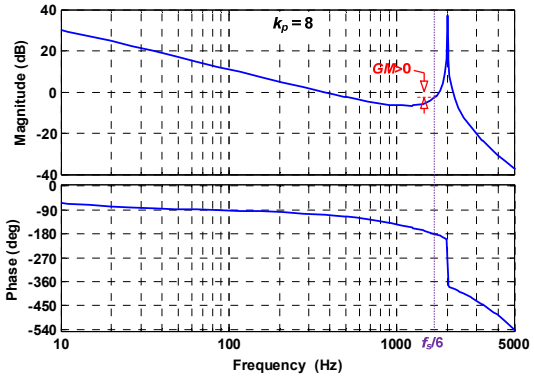

(a)

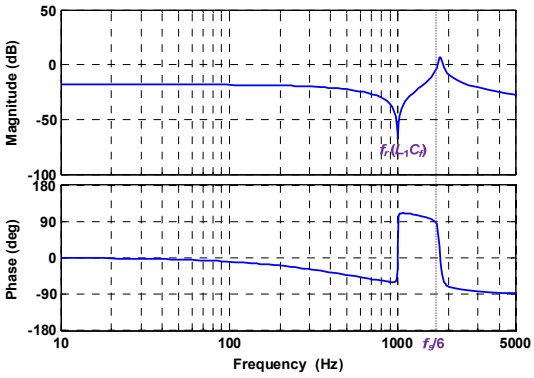

(b)

Fig. 7. Frequency responses of grid current control loop. (a) Open-loop gain T_2. (b) Closed-loop output admittance Y_{2c}.

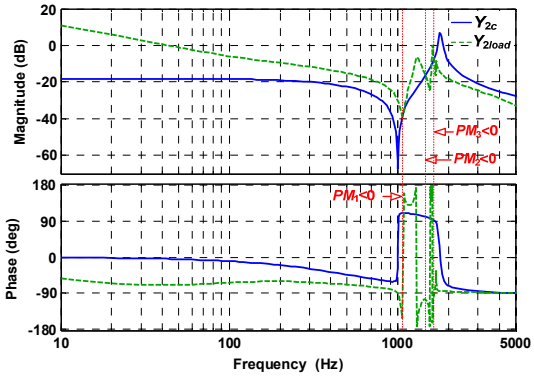

Fig. 8. Frequency responses of the closed-loop output admittance Y_{2c} and the equivalent load admittance Y_{2load}.

control system [8]. Fig. 7 (b) shows that the phase of Y_{2c} is out of [-90°, 90°] between the resonance frequency of L_1 and C_f and $f_s/6$, which agrees with the analysis in (10). This range is therefore the frequency region that the current control may be destabilized when it interacts with the resonant grid.

Fig. 8 compares the frequency responses for the closed-loop output admittance Y_{2c} and the load admittance Y_{2load}. It is seen that multiple resonance frequencies are introduced in the load admittance Y_{2load}, due to the interactions among the other three converters and cables. Moreover, in the frequency region that Y_{2c} has a negative real part, multiple intersections of their magnitude responses result in unstable oscillations at different frequencies. Hence, instead of the single resonance like in the *LCL* filter itself, as shown in Fig. 5, the resonant interactions of paralleled converters and cables may lead to unstable oscillations at multiple frequencies.

IV. Proposed Control Approach

A. Control Structure

Fig. 9 illustrates the block diagrams of the proportional derivative based stabilizing control methods in the discrete *z*-domain. The approach is based on the single current control loop, where the basic idea is to use the derivative controller to compensate the phase lag induced by the computation and PWM delays, and thus restrict the frequency region where the closed-loop output admittance has negative conductance.

Fig. 9 (a) shows the proposed controller for the converter current control loop, where an additional zero compensation is introduced with the backward Euler derivative controller, in order to improve the passivity property of the control loop. Fig. 9 (b) depicts the proposed controller for the grid current control loop, where the backward Euler derivative controller is used with a positive feedback.

Consequently, the open-loop gains of the current control loops can be derived in the following

$$T_{1d}(z) = \left[k_p + (k_{pd} - k_{dd}z^{-1})(1-z^{-1})\right] z^{-1}\mathrm{ZOH}\left\{Y_{1p}(s)\right\} \tag{13}$$

$$T_{2d}(z) = \left[k_p - k_d(1-z^{-1})\right] z^{-1}\mathrm{ZOH}\left\{Y_{2p}(s)\right\} \tag{14}$$

where $T_{1d}(z)$ and $T_{2d}(z)$ are the open-loop gains of converter and grid current control loops with the derivative controllers respectively. The resonant controller gain k_i is neglected. The PWM delay is included by performing the Zero-Order Hold (ZOH) transformation on the "plants" of control loops.

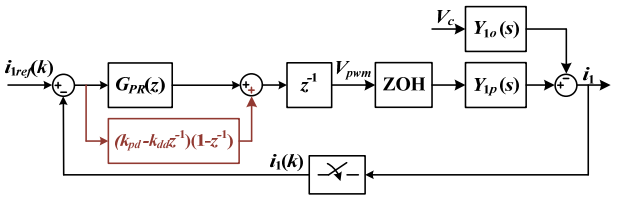

(a)

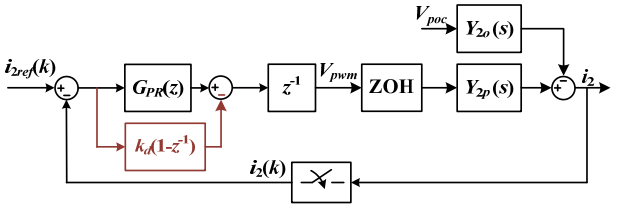

(b)

Fig. 9. Proportional derivative based stabilizing control strategy for grid converters. (a) Converter current control. (b) Grid current control.

B. Passivity-Based Desgin

The passivity-based design of the proposed controllers is illustrated in the following:

1) The root locus analyses based on (13) and (14) are used to design for a stable terminal behavior, i.e. Y_{1c} and Y_{2c} have no RHP poles.

2) Substituting $e^{-T_s s}$ for z^{-1} in Fig. 9, and replacing k_p in (9) and (10) by proposed controllers, then selecting controller parameters for passivity.

Fig. 10 shows the closed-loop pole trajectory of converter current control loop with the different k_{pd} in the derivative controller. The ratio k_{dd}/k_{pd} is swept from 0.2 to 2 with a step of 0.2. The proportional gain of the PR controller k_p is the same as Fig. 5. It is shown that the converter current control seen from the filter capacitor can be designed stable with the derivative controller. The stable limit of k_{pd} is decreased as the increase of k_{dd}/k_{pd}, and the maximum k_{pd} for k_{dd}/k_{pd}=2 is corresponding to 10.4.

Then, replacing k_p in (9) by the derivative controller, the passivity of control loop can be analyzed based on (15).

$$\mathrm{Re}\left\{\frac{1}{Y_{1d}}\right\}=(k_p+k_{pd})\cos(1.5T_s\omega)-(k_{pd}+k_{dd})\cos(2.5T_s\omega)+k_{dd}\cos(3.5T_s\omega) \tag{15}$$

Fig. 11 shows the influence of k_{dd}/k_{pd} on the passivity of the converter current control. Three different ratios of k_p/k_{pd} are compared. It is seen that at low k_p/k_{pd}, two frequency regions with negative $\mathrm{Re}\{Y_{1c}\}$ are caused by increasing k_{dd}/k_{pd}, while at the high k_p/k_{pd}, only the high frequency region with the negative $\mathrm{Re}\{Y_{1c}\}$ is left, but the frequency region with non-negative $\mathrm{Re}\{Y_{1c}\}$ is reduced to be below $0.3f_s$. Thus, there is a compromise in selecting k_p/k_{pd}. Moreover, the increase of k_{dd}/k_{pd} will enlarge the frequency region of the non-negative $\mathrm{Re}\{Y_{1c}\}$, but it also reduces the allowed k_p/k_{pd} for stability, as illustrated in Fig. 10. Hence, a trade-off is made by selecting k_p/k_{pd} =1, and k_{dd}/k_{pd} =1.4 in this work, for which the corresponding closed-loop poles are specified in Fig. 10.

The root locus analysis of grid current control loop based on (14) is shown in Fig. 12. The ratio k_d/k_p is swept from 0

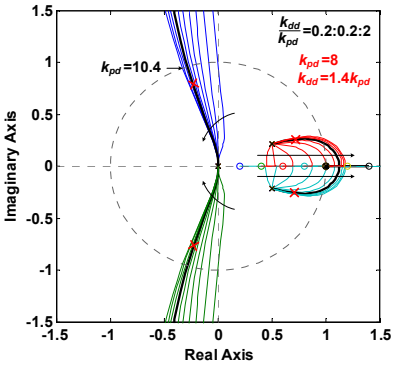

Fig. 10. Closed-loop pole trajectory of converter current control loop.

to 2.1 with a step of 0.3. A stable grid current control loop with the derivative controller in a positive feedback can be observed. Similarly to (15), k_p in (10) is substituted by the proportional derivative controller, which is then given by

$$\mathrm{Re}\left\{\frac{1}{Y_{2d}}\right\}=\frac{f\left(k_d/k_p\right)}{1-L_1C_f\omega^2} \tag{16}$$

$$f\left(k_d/k_p\right)=(1-k_d/k_p)\cos(1.5T_s\omega)+k_d\cos(2.5T_s\omega)/k_p$$

Unlike the converter current control, the passivity of grid current control is not only dependent on the ratio k_d/k_p, but also affected by the resonance frequency between L_1 and C_f, $f_r\,(L_1C_f)$. Hence, to enlarge the frequency region of passivity, k_d/k_p should be designed that yields the positive $f\,(k_d/k_p)$ for the frequencies lower than $f_r\,(L_1C_f)$, and the negative $f\,(k_d/k_p)$ for the frequencies above $f_r\,(L_1C_f)$.

Fig. 13 plots $f(k_d/k_p)$ in terms of k_d/k_p. It is seen that the frequency region of $f(k_d/k_p) \le 0$ is shift to the left as the increase of k_d/k_p. This implies that the frequency region with negative $\mathrm{Re}\{Y_{2c}\}$in Fig. 8 can be eliminated, provided that the lowest frequency of $f(k_d/k_p) \le 0$ is higher than $f_r\,(L_1C_f)$. On the other hand, the highest frequency of $\mathrm{Re}\{Y_{2c}\}\ge 0$ is also reduced. Hence, k_d/k_p is selected as 0.9 according to Fig. 13 for a good compromise, while k_p is selected as 9 for a proper damping of transient response based on Fig. 12.

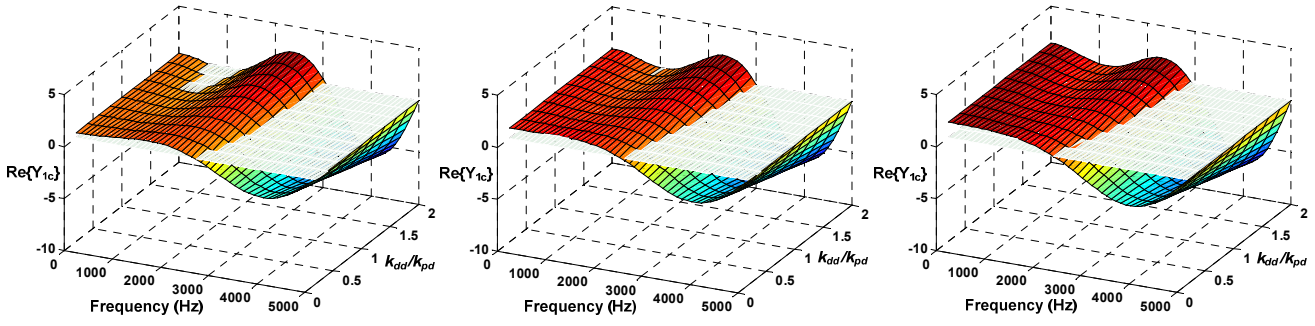

Fig. 11. Passivity analysis of converter current control. (a) k_p/k_{pd}= 0.5. (b) k_p/k_{pd}= 1. (c) k_p/k_{pd}= 1.5.

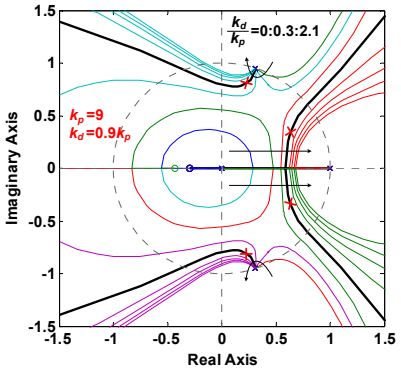

Fig. 12. Closed-loop pole trajectory of grid current control loop.

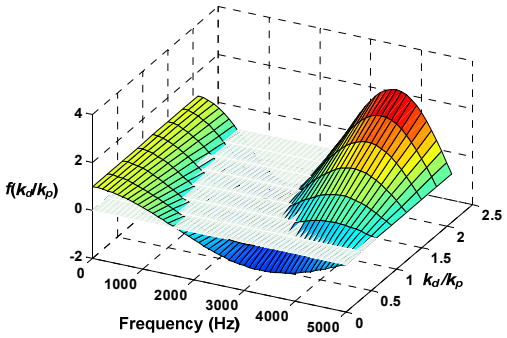

Fig. 13. Influence of k_d/k_p on the nominator of (16), denoted as $f(k_d/k_p)$.

C. Stabilizing Effect of Proposed Controller

Substituting $e^{-T_s s}$ for z^{-1} in Fig. 9, the stabilizing effect of proposed controllers can then be assessed by the impedance-based analysis. Fig. 14 plots the frequency responses of the closed-loop output admittances of converters and equivalent load admittances after including the proposed controllers. It is shown that the system keeps stable for both converter and grid current control with the proposed controllers. From Fig. 14 (a), it is seen that Y_{1c} has a phase out of [-90°, 90°] at the frequencies closed to $0.3f_s$, which matches with Fig. 11 (b). Compared to Fig. 8, Fig. 14 (b) gives an enlarged frequency region of passivity, which stabilizes the system.

V. Simulation and Experimental Results

A. Simulation Results

To confirm the theoretical analysis and the performance of the proposed controllers, time-domain simulations for the system shown in Fig. 1 are carried out within Simulink and Plecs blockset.

Fig. 15 shows the simulated grid currents of converters with converter current control, where the proposed controller is disabled at the time instant of 0.26 s. It can be seen that the system is destabilized by the interactions among converters.

Fig. 16 shows the simulated grid currents of converters with grid current control. Similarly, the derivative controller is disabled at the time instant of 0.26 s, and the system turns into unstable thereafter.

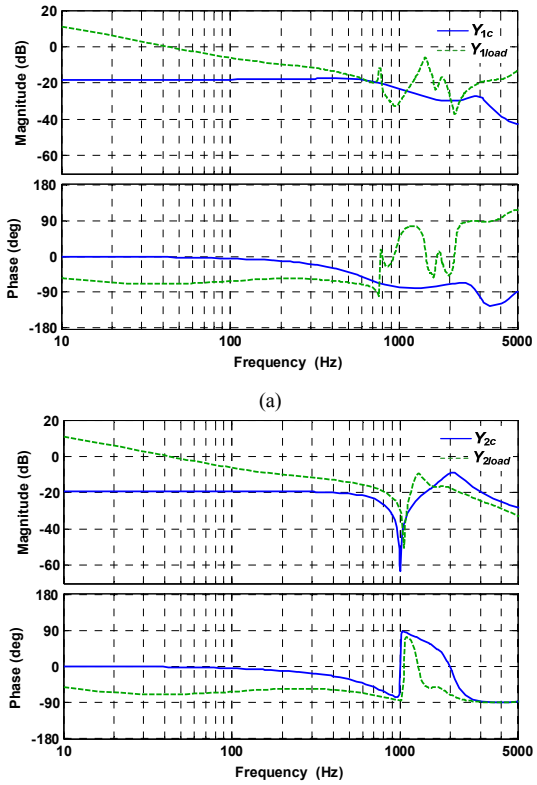

Fig. 14. Frequency responses of the converters output admittances Y_{1c} and Y_{2c}, and the equivalent load impedances Y_{1load} and Y_{2load} with the proposed controllers. (a) Converter current control. (b) Grid current control.

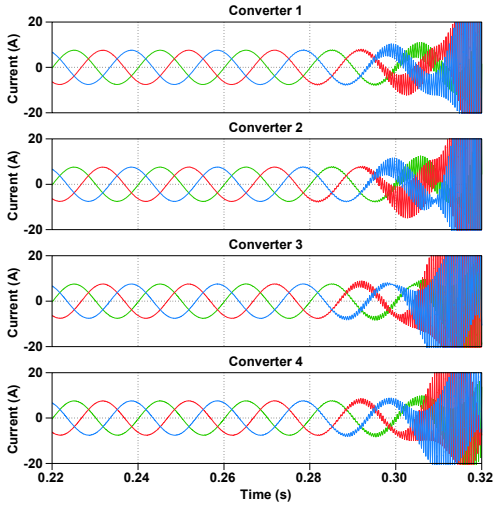

Fig. 15. Simulated grid currents of converters with converter current control.

B. Experimental Results

The laboratory tests on two paralleled grid converters are implemented, where a *California Instruments* MX-series AC power supply is used for grid emulation. The control system is implemented with a *dSPACE* DS1006 system.

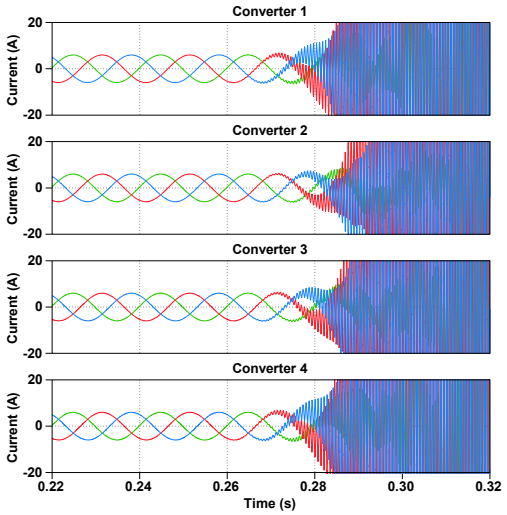

Fig. 16. Simulated grid currents of converters with grid current control.

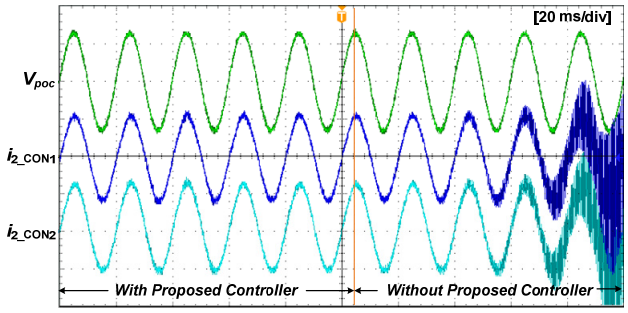

Fig. 17. Measured PoC voltage and grid currents of paralleled converters with converter current control. i_2: [5 A/div]. V_{pcc}: [250 V/div].

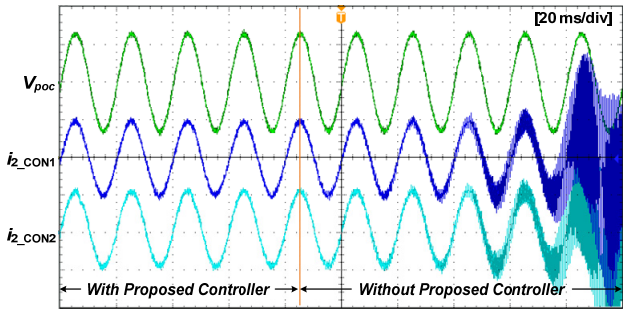

Fig. 18. Measured PoC voltage and grid currents of paralleled converters with grid current control. i_2: [5 A/div]. V_{pcc}: [250 V/div].

Fig. 17 shows the tested PoC voltage and grid currents of converters with the converter current control loop, while the measured results for grid current control is presented in Fig. 18. It is obvious that the system turns into unstable when the proposed controllers are disabled in experiments.

VI. CONCLUSIONS

This paper has analyzed the resonant interactions among the current control of grid converters and cables. It has been shown that the phase lag induced by system delays result in negative conductance at the PoC of converters, which may destabilize the system. Two proportional derivative control schemes have been designed for the passivity of converter and grid current control loops respectively. Simulations and experimental results have been shown that the phase lead of derivative control action improves the passivity of control systems, and thus stabilize the system.

REFERENCES

[1] J. Agorreta, M. Borrega, J. Lopez, and L. Marroyo, "Modeling and control of *N*-paralleled grid-connected inverters with *LCL* filter coupled due to grid impedance in PV plants," *IEEE Trans. Power Electron*., vol. 26, no. 3, pp. 770-785, Mar. 2011.

[2] Z. Shuai, D. Liu, J. Shen, C. Tu, Y. Cheng, and A. Luo, "Series and parallel resonance problem of wideband frequency harmonic and its elimination strategy," *IEEE Trans. Power Electron.*, vol. 29, no. 4, pp. 1941-1952, Apr. 2014.

[3] X. Wang, F. Blaabjerg, and W. Wu, "Modeling and analysis of harmonic stability in an AC power-electronics-based power system," *IEEE Trans. Power Electron.*, vol. PP, no. 99, pp. 1-12, Feb. 2014.

[4] S. Zhang, S. Jiang, X. Lu, B. Ge, and F. Z. Peng, "Resonance issues and damping techniques for grid-connected inverters with long transmission cable," *IEEE Trans. Power Electron*., vol. 29, no. 1, pp. 110-120, Jan. 2014.

[5] L. Harnefors, M. Bongiorno, and S. Lundberg, "Input-admittance calculation and shaping for controlled voltage-source converters," *IEEE Trans. Ind. Electron*., vol. 54, no. 6, pp. 3323-3334, Dec. 2007.

[6] L. Harnefors, L. Zhang, and M. Bongiorno, "Frequency-domain passivity-based current controller design," *IET Power Electron.*, vol. 1, no. 4, pp. 455-465, Dec. 2008.

[7] R. N. Beres, X. Wang, F. Blaabjerg, C. L. Bak, and M. Liserre, "A review of passive filters for grid-connected voltage source converters," in *Proc. IEEE APEC* 2014, pp. 2208-2215.

[8] X. Wang, F. Blaabjerg, and P. C. Loh, "Design-oriented analysis of resonance damping and harmonic compensation for LCL-filtered votlage source converters," in *Proc. IEEE IPEC* 2014, pp. 216-223.

[9] F. Fuchs, D. V. Pham, and A. Mertens, "Analysis of grid current control in consideration of voltage-feedforward and cable capacitance demonstrated on a fully sized wind turbine installed in a wind park," in *Proc. ECCE* 2013, pp. 3325-3332.

[10] J. Dannehl, M. Liserre and F. Fuchs, "Filter-based active damping of voltage source converters with *LCL* filter," *IEEE Trans. Ind. Electron.*, vol. 58, no. 8, pp. 3623-3633, Aug. 2011.

[11] T. Messo, J. Jokipii, J. Puukko, and T. Suntio, "Determining the value of DC-link capacitance to ensure stable operation of a three-phase photovoltaic inverter," *IEEE Trans. Power Electron.*, vol. 29, no. 2, pp. 665-673, Feb. 2014.

[12] T. Messo, J. Jokipii, A. Makinen, T. Suntio, "Modeling the grid synchronization induced negative-resistor-like behavior in the output impedance of a three-phase photovoltaic inverter," in *Proc. IEEE PEDG* 2013, pp.1-8.

[13] B. Wen, D. Boroyevich, P. Mattavelli, Z. Shen, and R. Burgos, "Experimental verification of the generalized Nyquist stability criterion for balanced three-phase AC systems in the presence of constant power loads," in *Proc. IEEE ECCE* 2012, pp. 3926-3933.

[14] S. Buso and P. Mattavelli, *Digital Control in Power Electronics*, San Francisco, CA: Morgan & Claypool Publ., 2006.

[15] O. Brune, " Synthesis of a finite two-terminal network whose driving-point impedance is a prescribed function of frequency," MIT, Journ. Math. Phy. vol. 10, pp. 191-236, 1931.

[16] A. Riccobono and E. Santi, "A novel passivity-based stability criterion (PBSC) for switching converter DC distribution systems," in *Proc. IEEE APEC* 2012, pp. 2560-2567.